TEXTURES AND FRAGMENT SIZE DISTRIBUTIONS IN DIOGENITE (HED) METEORITES: PROCESSES AND GEOLOGICAL SETTINGS. E.R. McLeish[1] and A.H. Treiman[2]. [1]University College London, Gower St., London, WC1H 6BT, England. [2]Lunar and Planetary Institute, Houston, TX 77058, USA <treiman@lpi.usra.edu>.

Brecciated diogenite meteorites occur in two textural patterns: fragmental and granular. Fragmental diogenites consist of angular clasts, lightly annealed or cemented together. Sizes of these fragments follow a power-law distribution (i.e., are scale-invariant). Granular diogenites are compact rocks, with shear boundaries between their fragments. Fragmental diogenites are impact ejecta; granular diogenites are likely to be basement rock, deformed during impacts.

Diogenites, basaltic achondrites of the howardite-eucrite-diogenite (HED) clan, are orthopyroxenites with minor chromite, olivine, and other phases. They are inferred be from the asteroid 4-Vesta [1,2,3].

SAMPLES AND METHODS

We investigated several Antarctic diogenites: ALHA77256,53; ALH85015,4; EETA79002,22; EET83246,12; EET83247,13; EET87530,12; GRA98108,15; LAP91900,19; LEW88008,13; LEW88679,5; PCA92077,7; and TIL82410,17. Thin sections were studied optically at LPI, and with secondary electron and backscattered electron petrography (SEI and BSE) at Johnson Space Center (JEOL JSM-5910). Length measurements on digital images were acquired with the computer program Digital Micrograph® 2.5.

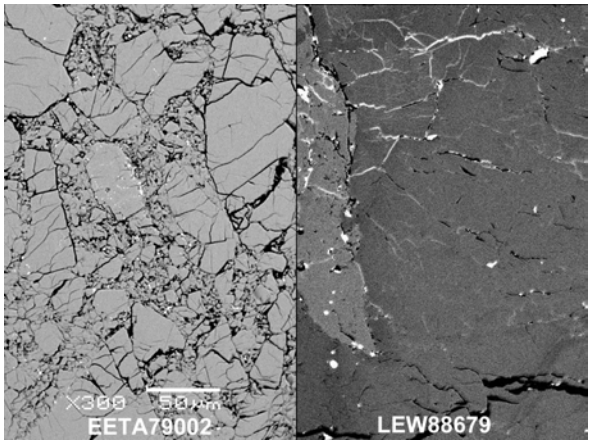

Fig. 1. Fragmental texture (left) and granular texture (right). BSE images, same scale. View at right includes several pyroxene grains and an olivine (lighter tone), with no void space between the grains.

TEXTURES

The diogenites studied were of two textural patterns: granular and fragmental (Fig. 1). In granular-textured diogenite, distinct pieces of diogenite rock abut directly on each other, or are separated by linear (or curvilinear) fine-grained bands of granular textured material. Minerals in these rock pieces have polygonised extinction, suggestive of significant strain. ALHA77256, ALH85015, GRA98108, and LEW88679 have granular textures, as does the Martian meteorite ALH84001 [4].

The other diogenites here have fragmental textures – angular rock and mineral fragments set among smaller similar fragments. The smallest fragments are variably annealed or sintered together. SEI and BSE images of fragmental diogenites appear similar over a range of magnifications (Fig. 2). In other words, their fragment size distribution appears scale-invariant.

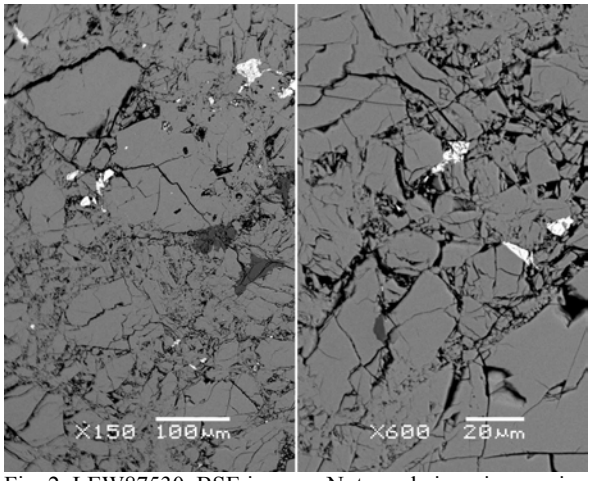

Fig. 2. LEW87530, BSE images. Note scale invariance – i.e. similarity of images at different magnifications. Bright grains are chromite, dark gray grains are plagioclase.

FRAGMENTAL DIOGENITES

Grain size distributions for EETA79002,22 and LAP91900,19 were determined from BSE images. The former was analysed from one representative image at 550x. LAP91900 was analysed from a representative images at 300x and a subframe at 1800x, chosen to highlight its fragmental texture. The subframe and its magnification were chosen so that the grains smaller than a few microns could be counted. To determine grain size distributions, each grain in an image was tagged and its length was measured, as was the longest width perpendicular to this length. An objective measure of grain size, **r**, was calculated as the square root of the product of the length and the width. This two-dimensional sample is assumed to represent the whole meteorite because the grains orientations and the thin section plane are effectively random. Grain sizes **r** were sorted into data bins of fixed size ratio and plotted as cumulative number of grains larger than **r** per unit area, **N(>r)**, versus **r** on logarithmic scales (Fig. 3).

INTERPRETATION

It can be seen in Figure 3 that the cumulative size distributions for fragments in these diogenites follow straight lines over significant ranges of **r**:

$$\log\{N(>r)\} = -D \cdot \log(r) + a, \quad \text{or}$$
$$N(>r) = a \cdot r^{-D} \qquad [eq.\ 1],$$

as shown in Figure 3 and predicted from fragmentation theory and simulations [5-11].

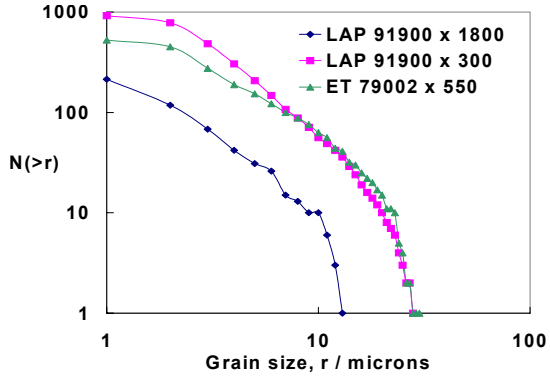

Fig. 3. Fragment frequency-size distributions for two diogenites.

This power-law relation of sizes implies scale-invariance, confirming the inference from visual inspection. Size distributions for the two LAP images do not have the same intercept in Fig. 3 (**a** in eq. 1), although their slopes **D** are similar. This difference in intercepts is an artefact – the 1800x image was chosen to show small-scale fragmental texture, and so oversamples the smaller sizes in the distribution.

The expected linearity of **log{N(>r)}** versus **log{r}** of Figure 3 does not obtain for the largest and smallest grains – both populations are low compared to that predicted from linearity. These deviations may be real, in part, but can also arise as artefacts of sampling and analysis. At the smallest sizes, the deviation from linearity could represent three effects. (1) BSE images do not represent the smaller grains accurately because of focus and/or pixelation. (2) Small grains may be plucked out during thin section manufacture. (3) Annealing makes it difficult to distinguish small grains from each other (esp. in EETA79002). At the largest sizes, deviation from linearity can arise from the finite size of the images – one can only measure grains that fall wholly within an image, so large grains are under-represented.

Power law exponents **D** were determined by linear least-squares fitting (excluding the smallest and largest sizes): 1.96±0.07 for LAP at 300x; 1.42±0.07 for LAP at 1800x; and 1.33±0.06 for EET79002 at 550x. The latter curve rolls off to lower **N(>r)** at higher **r**, and can be fit as two linear segments: **D** = 1.06±0.02 for 2 < **r** < 10 μm; and **D** = 2.07±0.06 for 10 < **r** < 20 μm.

These power-law exponents are calculated for two-dimensional objects (really $\mathbf{D_{2d}}$), while most literature data are for three-dimensional objects. To convert from the latter to the former, in this case, $\mathbf{D_{2d} = D_{3d} - 1}$ [12]. Reported fragmental materials of many origins yield $\mathbf{D_{2d}}$ between 0.9 (crushed quartz) and 2.5 (ash and pumice) [7,9]; most fragmental assemblages have $\mathbf{D_{2d}}$ = 1.5±0.4 [10,11,13]. Our data for fragmental diogenites fall in this common range of $\mathbf{D_{2d}}$.

GEOLOGIC SETTING

The fragmental diogenites have been long interpreted as impact ejecta, and our investigation of their grain sizes confirms this inference. The similarity between the measured D_{2d} for the diogenites and those of pure fragmentation products suggests that the diogenite fragments have not been winnowed of fine material, as by aeolian processes. The relative paucity of large fragments is yet unexplained. It could be merely an artefact of our method, could relate to the structure of the precursor rock (i.e. original grain size or fragment sizes induced by a prior impact), or could mean that larger fragments are sorted out during fragmentation and emplacement to form fragmental diogenites. Granular diogenites formed in a different setting, as they are not merely annealed fragmental diogenites. They may represent bedrock from beneath impact craters [14], as has been inferred for the Martian meteorite ALH84001 [15].

Acknowledgements. This work was performed during a LPI Summer Internship to ERM, advised by AHT. Meteorite samples were loaned by the MWG and the Office of the Curator of Antarctic Meteorites, Johnson Space Center. C. Schwandt (Lockheed @ JSC) supported our SEM and EMP analyses. The C^2PDA at LPI are thanked for patient assistance with computers.

REFERENCES

[1] Drake M.J. (1979) *Asteroids* (eds. T. Gehrels and M.S. Matthews), p. 765. U. AZ Press. [2] Drake M.J. (2001) *MaPS* **36**, 501. [3] Keil K. (2002) in Asteroids III, (eds. W. Bottke et al.), p. 573. U. AZ Press. [4] Mittlefehldt D.W. (1994) *Meteoritics* **29**, 214. [5] Melosh H.J. et al. (1992) JGR 97, 14735. [6] Wohletz K. and Brown W. (1995) Los Alamos Nat'l. Lab. Rept. LA-UR95-0371. [7] Turcotte D.L. (1997) *Fractals and Chaos in Geology and Geophysics*, 398p. Cambridge University Press. [8] Turcotte D.L. (1986) *JGR* **91**, 1921. [9] Hartmann W.K. (1969) *Icarus* **10**, 201. [10] Klacka J. (1992) *Earth Moon Planets* **56**, 47. [11] Schoutens J.E. (1979) *Nuclear Geoplosics Sourcebook*, **55**, part 2, section 4, Rep. DNA OIH-4-2, Defence Nuclear Agency, cited in [8]. [12] Petersen T.D. (1996) *Contrib. Mineral. Petrol.* **124**, 395. [13] Fujiwara A. et al. (1977) *Icarus* **31**, 277. [14] French B.M. (1998) *Traces of Catastrophe*, Lunar and Planetary Institute, Houston. 122p. [15] Treiman A.H. (1998) *MaPS* **33**, 753.